Quantum versus semiclassical signatures of correlated triple ionization in Dalitz plots

Dmitry K. Efimov , Georgios P. Katsoulis , Tymoteusz Rozpętkowski , Sergiusz Chwałowski , Agapi Emmanouilidou , and Jakub S. Prauzner-Bechcicki , Institute of Theoretical Physics, Faculty of Fundamental Problems of Technology, Wrocław University of Science and Technology, 50-370 Wrocław, Poland

Department of Physics and Astronomy, University College London, Gower Street, London WCIE 6BT, England, United Kingdom Jagiellonian University in Kraków, Faculty of Physics, Astronomy and Applied Computer Science, Marian Smoluchowski Institute of Physics, Lojasiewicza 11, 30-348 Krakow, Poland



(Received 23 October 2024; accepted 20 June 2025; published 9 July 2025)

We investigate correlated three-electron escape in Ne when driven by an intense, infrared laser field. We do so by employing a reduced-dimensionality quantum-mechanical model and two three-dimensional semiclassical models. One semiclassical model is a recently developed one that accounts with effective Coulomb potentials for the interaction between two bound electrons (ECBB) while it fully accounts for all other interactions. The other semiclassical model is the Heisenberg one, which effectively accounts for the interaction of each electron with the core via a soft-core potential. We identify and compare the signatures of correlated three-electron escape for both quantum and semiclassical models on Dalitz plots and find a better agreement between the quantum and the ECBB model. We also show that a central "spot" on the Dalitz plots is reproduced by all models. Using the ECBB model we associate this spot with the direct triple ionization pathway and argue this to be the case also for the quantum model. Devising a simple classical model that accounts for the direct pathway of triple ionization, we show that the width of this spot in the Dalitz plots solely depends on the time of tunnel ionization.

DOI: 10.1103/43wt-x129

I. INTRODUCTION

Studies of interaction of strong laser fields with atoms and molecules brought out many intriguing phenomena: starting with above-threshold ionization, nonsequential multiple ionization, and high-harmonic generation, through attosecond pulse generation, initiating eventually a spectrum of new experimental techniques, just to mention attosecond streaking based measurements or attosecond transient spectroscopy [1]. Progress in experimental works has always been accompanied by a considerable effort aimed at the theoretical description of studied phenomena. Achieving the latter is still quite a challenge, especially when focusing on processes where more than two electrons are involved. Nonsequential multiple ionization (NSMI) is an excellent example. While the description of nonsequential double ionization may be considered settled [2–14], the description of triple ionization cannot be considered as such, regardless of the effort that has been put into addressing it [15–27]. Correlated multi-electron escape is a fundamental phenomenon, since it is mediated by Coulomb interaction. Combined with backscattering from the ion, an example of correlated two-electron escape is the well-known finger-like structure, which is exhibited in the correlated momenta distributions obtained experimentally and theoretically [8,9,28]. Concerning three-electron escape, correlation is not fully represented in the experimental data available, since they do not measure all three final electron momenta in coincidence [15–18]. In this work, we demonstrate correlation

in three-electron escape using the Dalitz or ternary plots. Their usefulness was first shown in the study of ion impact ionization [29–31]. The Dalitz plots were later introduced in strong-field triple ionization [26,27]. Here, we show that distributions visualized via Dalitz or ternary plots enable one to also infer the contribution of various triple ionization channels when combined with semiclassical calculations and, as such, open a way of interpretation of momentum distributions obtained in quantum-mechanical calculations and experiments.

There are several complementary theoretical approaches to the problem of multiple ionization. One may try to use the strong-field approximation, however, already for two electrons the calculation becomes very complicated, not mentioning inclusion of a third electron [32]. Next, one may use classical and semiclassical methods [14,19,21,22,33] or directly tackle the numerical solution of an appropriate Schrödinger equation [5,6,8,24,34–36]. In both, classical and quantum, approaches one either uses the full geometry of the problem or uses simplified models. Yet, in each case the singularity of the Coulomb potential poses a problem.

Out of the multitude of possible strong-field phenomena, here, we focus our attention on NSMI. In brief, NSMI is considered a three-step process [2]: (i) an electron tunnelionizes from the laser-field-lowered Coulomb potential, (ii) this electron is accelerated in the laser field and can return to rescatter from the parent ion and (iii) transfers energy to the bound electrons leading to multiple ionization. The first step is not allowed classically, therefore it is typically included via the quantum-mechanical Ammosov-Delone-Krainov formula [37,38] leading to a semiclassical approach. In modeling the second and the third steps, semiclassical methods are founded

^{*}Contact author: jakub.prauzner-bechcicki@uj.edu.pl

on solving the Hamilton's or Newton's equations of motion. In principle, for semiclassical methods, the number of active electrons is not as challenging as for quantum approaches, yet the Coulomb singularity in the electron-core interaction term is problematic. The latter allows an electron to acquire a negative energy of any value, which may be compensated via electron-electron interaction leading to the escape of another electron—a process known as unphysical or artificial autoionization. Therefore, one introduces the soft-core Coulomb-like potentials [39] or Heisenberg potentials [40,41] as a remedy. Let us clarify, the Heisenberg potential (H model) effectively leads to softening of the Coulomb singularity [33,42]. However, softening the Coulomb potential in classical models does not accurately describe electron scattering from the core [43,44]. One way to address this is to fully account for the Coulomb interaction of each electron with the core as well as for the Coulomb interaction between any pair of electrons that are not both bound. In this case, effective Coulomb potentials are used to account for the interaction of a bound-bound electron pair (ECBB model) [33].

The quantum-mechanical approach includes all three steps of the process by default, however, increasing the number of electrons involved becomes a formidable task, especially when the Schrödinger equation is solved on a grid. Therefore, full-dimensional quantum calculations on a grid have been performed only for two electrons and for a specific range of parameters of the laser pulse (i.e., frequency, field amplitude, phase, envelope) [6,8,34,45,46]. Models incorporating reduced geometries are used to allow greater flexibility concerning the parameters of the laser pulses and the number of electrons involved [5,24,35,36,47]. In these models, typically, each of the electrons is allowed to move along a one-dimensional track. Combined with the use of the softcore Coulomb-like potential these models make the problem computationally tractable. Using the value of the soft-core parameter to adjust the ionization energy is an additional benefit of such an approach.

In the following we use both semiclassical and quantum approaches to describe triple ionization of atoms in strong laser fields. Our goal is to study "fingerprints" of correlated electron escape found in the final momenta of the escaping electrons. Collecting experimental data for triple and higher ionization is still a difficult task when it comes to measuring momenta of all electrons and the nucleus; it may be feasible in the future [13,48–53]. To visualize the momenta of the three outgoing electrons and identify the electron-electron correlations, we map all relevant events onto Dalitz plots [26,27,29–31]. We find that a middle spot in the Dalitz plots of the electron momenta is a fingerprint of correlated electron-escape which is reproduced in a consistent manner regardless of the approach taken, i.e., semiclassical or quantum.

The paper is structured as follows, first, we briefly introduce the semiclassical and quantum models employed in this work. Then, we discuss the obtained electron momenta distributions in the context of Dalitz plots and compare the semiclassical with the quantum results. Next, we examine signatures of direct ionization, i.e., simultaneous emission of all three electrons following recollision, in the Dalitz plots. We identify a spot in the middle of Dalitz plots as a signature

of direct ionization. Very importantly, we devise a simple classical model to explain the width of this spot and connect this width with the time the recolliding electron tunnel-ionizes through the field-lowered Coulomb potential.

II. DESCRIPTION OF THE MODELS

A. Classical models

We employ two three-dimensional (3D) semiclassical models of NSMI developed in the nondipole framework, accounting for the motion of the core and the three electrons. In what follows, we describe the formulation of the ECBB model and the H model that address multi-electron escape in strongly driven atoms. The two methods resolve in a different way unphysical autoionization in 3D semiclassical models that fully account for the Coulomb singularity, with the ECBB model having better agreement with experiment [42].

1. Effective Coulomb potential method

The cornerstone of the effective-Coulomb-potential model [33,42] is the exact treatment of the two interactions that we consider the most important during a recollision. Namely, we account for the full Coulomb potential between each electron, bound or quasifree, and the core. Quasifree refers to a recolliding electron or an electron escaping to the continuum. We also treat the exact Coulomb potential, and hence the exact energy transfer between any pair of a quasifree and a bound electron. To tackle the problem of artificial autoionization, we take a different approach to softening the Coulomb potential. Specifically, we use effective Coulomb potentials to account for the interaction of a bound-bound electron pair (ECBB), i.e., we approximate the energy transfer from a bound to another bound electron. Hence, we expect the ECBB model to be more accurate for laser pulse parameters where multi-electron ionization due to transfer of energy between electrons in excited states after recollisions plays less of a role. A sophisticated element of the ECBB model is its ability to classify an electron as quasifree or bound on the fly during time propagation. That is, we decide on the fly if the interaction between a pair of electrons will be described by the full or an effective Coulomb potential. To do so, we use a set of simple criteria detailed

The Hamiltonian of the three-electron atom is given by

$$H = \sum_{i=1}^{4} \frac{\left[\tilde{\mathbf{p}}_{i} - Q_{i}\mathbf{A}(y, t)\right]^{2}}{2m_{i}} + \sum_{i=2}^{4} \frac{Q_{i}Q_{1}}{|\mathbf{r}_{1} - \mathbf{r}_{i}|} + \sum_{i=2}^{3} \sum_{j=i+1}^{4} \left[1 - c_{i,j}(t)\right] \frac{Q_{i}Q_{j}}{|\mathbf{r}_{i} - \mathbf{r}_{j}|} + \sum_{i=2}^{3} \sum_{j=i+1}^{4} c_{i,j}(t) \times \left\{V_{\text{eff}}\left[\zeta_{j}(t), |\mathbf{r}_{1} - \mathbf{r}_{i}|\right] + V_{\text{eff}}\left[\zeta_{i}(t), |\mathbf{r}_{1} - \mathbf{r}_{j}|\right]\right\}, \quad (1)$$

where Q_i is the charge, m_i is the mass, \mathbf{r}_i is the position vector and $\tilde{\mathbf{p}}_i$ is the canonical momentum vector of particle *i*. The mechanical momentum \mathbf{p}_i is given by

$$\mathbf{p}_i = \tilde{\mathbf{p}}_i - Q_i \mathbf{A}(\mathbf{y}, t), \tag{2}$$

where $\mathbf{A}(y,t)$ is the vector potential and $\mathbf{E}(y,t) = -\partial \mathbf{A}(y,t)/\partial t$ is the electric field. The effective Coulomb potential that an electron i experiences at a distance $|\mathbf{r}_1 - \mathbf{r}_i|$

from the core (particle 1 with $Q_1 = 3$), due to the charge distribution of electron j is derived as follows [33,54]: We approximate the wave function of a bound electron j with a 1s hydrogenic wave function

$$\psi(\zeta_j, |\mathbf{r}_1 - \mathbf{r}_j|) = \left(\frac{\zeta_j^3}{\pi}\right)^{1/2} e^{-\zeta_j |\mathbf{r}_1 - \mathbf{r}_j|},\tag{3}$$

with ζ_j the effective charge of particle j [33,54]. The reason we choose the 1s hydrogenic wave function to describe electron j is that it leads to a simple expression for the charge distribution and in turn for the effective potential that electron j creates, as we show in what follows. Hence, using Gauss's law, one finds that the potential produced due to the charge distribution $-|\psi(\zeta_i, |\mathbf{r}_1 - \mathbf{r}_i|)|^2$ is given by

$$V_{\text{eff}}(\zeta_j, |\mathbf{r}_1 - \mathbf{r}_i|) = \frac{1 - (1 + \zeta_j |\mathbf{r}_1 - \mathbf{r}_i|) e^{-2\zeta_j |\mathbf{r}_1 - \mathbf{r}_i|}}{|\mathbf{r}_1 - \mathbf{r}_i|}, \quad (4)$$

with ζ_i the effective charge of particle j [33,54]. When $\mathbf{r}_i \rightarrow$ ${\bf r}_1$, the effective potential is equal to ζ_i , hence ensuring a finite energy transfer between bound electrons i and j. As a result no artificial autoionization takes place. The functions $c_{i,j}(t)$ determine at time t during propagation whether the full Coulomb or effective $V_{\text{eff}}(\zeta_i, |\mathbf{r}_1 - \mathbf{r}_i|)$ and $V_{\text{eff}}(\zeta_i, |\mathbf{r}_1 - \mathbf{r}_i|)$ potentials describe the interaction between electrons i and j [33]. The effective potentials are activated only when both electrons in a pair are bound. The simple criteria we use to determine if an electron is bound or quasifree is as follows: A quasifree electron can transition to bound following a recollision. Specifically, after a quasifree electron has its closest approach to the core, it is considered bound if its position along the z axis is influenced more by the core than the electric field. Specifically, we check if the position of the electron along the electric field, i.e., z axis here, has at least two extrema of the same kind, i.e., two maxima or two minima, in a time interval less than half a period of the laser field. At the time when the second extremum is identified in the position of the electron along the electric field, this electron is registered as bound [33]. On the other hand, a bound electron can transition to quasifree due to transfer of energy during a recollision or from the laser field. In the former case, a bound electron becomes quasifree if its potential energy with the core constantly decreases following recollision. A bound electron can also transition to quasifree due to the laser field if its energy becomes and remains positive. The criteria are discussed in detail and illustrated in Ref. [33].

We use a vector potential of the form

$$\mathbf{A}(y,t) = -\frac{E_0}{\omega} \exp\left[-2\ln(2)\left(\frac{ct-y}{c\tau}\right)^2\right] \sin(\omega t - ky)\hat{\mathbf{z}},$$
(5)

where $k = \omega/c$ is the wave number of the laser field. The direction of the vector potential and the electric field is along the z axis, while the direction of light propagation is along the y axis. The magnetic field, $\mathbf{B}(y,t) = \mathbf{V} \times \mathbf{A}(y,t)$, points along the x axis. The pulse duration is $\tau = 25$ fs, while the wavelength is 800 nm. For Ne, we consider intensities 1.0, 1.3 and 1.6 PW/cm². The highest intensity considered here is chosen such that the probability for a second electron to tunnel ionize solely due to the laser field is very small

[42]. Hence, electron-electron correlation prevails in triple ionization, with the bound electrons ionizing only due to recollisions. One electron tunnel ionizes through the fieldlowered Coulomb barrier at time t_0 along the direction of the total laser field. Tunneling occurs with a nonrelativistic quantum-mechanical tunneling rate described by the instantaneous Ammosov-Delone-Krainov (ADK) formula [37,38] with the empirical corrections by Tong and Lin for high intensities [55]. Using this formula, we obtain a rate that also accounts for depletion of the initial ground state [42]. We find the time t_0 in the time interval $[-2\tau, 2\tau]$ where the electric field is nonzero, using importance sampling [56], with τ the full width at half maximum of the pulse duration in intensity. The exit point of the recolliding electron along the direction of the electric field is obtained analytically using parabolic coordinates [57]. The electron momentum along the electric field is set equal to zero, while the transverse one is given by a Gaussian distribution. This distribution represents the Gaussian-shaped filter with an intensity-dependent width arising from standard tunneling theory [38,58,59]. For the initially bound electrons, we employ a microcanonical distribution [33], while the core is initially at rest.

In our formulation, we fully account for the Coulomb singularities. Hence, an electron can approach infinitely close to the nucleus during time propagation. To ensure the accurate numerical treatment of the *N*-body problem in the laser field, we perform a global regularization. This regularization was introduced in the context of the gravitational *N*-body problem [60]. To integrate Hamilton's equations of motion, we use a leapfrog technique [61,62] jointly with the Bulirsch-Stoer method [63,64]. This leapfrog technique allows integration of Hamilton's equation when the derivatives of the positions and the momenta depend on the quantities themselves. The steps involved in this technique, employed in this work, are described in detail in Ref. [33].

2. Heisenberg potential method

An alternative approach for excluding unphysical autoionization in 3D semiclassical treatments is adding a Heisenberg potential for the interaction of each electron with the nucleus [40]. This amounts to adding a potential barrier that mimics the Heisenberg uncertainty principle and prevents each electron from a close encounter with the nucleus. The advantage of this model is that it describes electronic interactions via Coulomb forces at all times during time propagation. However, the reduction of the phase space that each electron can access does not accurately describe the interaction of each electron with the nucleus, leading to "softer" recollisions upon the return of the recolliding electron to the core [33].

The Heisenberg potential, originally proposed by Kirschbaum and Wilets in Ref. [40], is given by

$$V_{H,i} = \frac{\xi^2}{4\alpha\mu r_{i,1}^2} \exp\left\{\alpha \left[1 - \left(\frac{r_{i,1}p_{i,1}}{\xi}\right)^4\right]\right\},\tag{6}$$

where $\mathbf{r}_{i,1} = \mathbf{r}_1 - \mathbf{r}_i$ is the relative position of each one of the three electrons i = 2, 3, 4 with respect to the core $i = 1, \mathbf{p}_{i,1}$

is the corresponding relative momentum,

$$\mathbf{p}_{i,1} = \frac{m_i \mathbf{p}_1 - m_1 \mathbf{p}_i}{m_1 + m_i},\tag{7}$$

and $\mu = m_1 m_i / (m_i + m_1)$ is the reduced mass of the electron core system. This potential restricts the relative position and momentum of electron *i* according to

$$r_{i,1}p_{i,1} \geqslant \xi. \tag{8}$$

Hence, the Heisenberg potential acts as a repulsive potential when the electron is close to the nucleus. Including the Heisenberg potential for all electron-core pairs, we find that the Hamiltonian is given by

$$H = \sum_{i=1}^{4} \frac{\left[\tilde{\mathbf{p}}_{i} - Q_{i}\mathbf{A}(y, t)\right]^{2}}{2m_{i}} + \sum_{i=1}^{3} \sum_{j=i+1}^{4} \frac{Q_{i}Q_{j}}{|\mathbf{r}_{i} - \mathbf{r}_{j}|} + \sum_{i=2}^{4} V_{H,i}.$$
(9)

B. Quantum model

The numerical treatment of three-electron atoms in a complete configuration space poses a significant challenge. We employ a model with restricted dimensionality capable of capturing the core dynamics of electrons in a strong field [19,24]. In this model, each electron moves along a one-dimensional (1D) track inclined at a constant angle α with respect to the laser pulse's polarization axis ($\tan \alpha = \sqrt{2/3}$). The tracks form a constant angle of $\pi/6$ between each pair. This geometry is determined through a local stability analysis of the adiabatic full-dimensional potential [19,65,66] and has been successfully applied in previous studies of three-electron dynamics [24–26,67–69].

The Hamiltonian is given by

$$H = \sum_{i=1}^{3} \frac{p_i^2}{2} + V + V_{\text{int}}, \tag{10}$$

where V and $V_{\rm int}$ represent the atomic and interaction potentials, respectively. The atomic potential in the restricted space is expressed as

$$V = -\sum_{i=1}^{3} \frac{3}{\sqrt{r_i^2 + \epsilon^2}} + \sum_{i,j=1; i < j}^{3} \frac{q_{ee}^2}{\sqrt{(r_i - r_j)^2 + r_i r_j + \epsilon^2}},$$
(1)

with a smoothing factor $\epsilon = \sqrt{0.83}$ and an effective charge $q_{ee} = 1$ to reproduce the triple ionization potential of the neon atom $(I_p = 4.63 \text{ a.u.})$. The interaction term is described as

$$V_{\text{int}} = \sqrt{\frac{2}{3}} A(t) \sum_{i=1}^{3} p_i,$$
 (12)

where the vector potential is defined as

$$A(t) = \frac{F_0}{\omega} \sin^2 \left(\frac{\pi t}{T_n}\right) \sin \left(\omega t + \phi\right)$$

for $t \in [0, T_p]$. The laser pulse parameters are field amplitude F_0 ; carrier frequency $\omega = 0.06$ a.u.; pulse length $T_p = 2\pi n_c/\omega$; number of optical cycles, $n_c = 3$; and carrier-envelope phase ϕ set to zero.

To study the interaction of three-electron atoms with a laser pulse, we need a wave function describing the motion of three electrons (assuming the nucleus is infinitely heavy). The wave function is composed of spatial and spin parts and requires antisymmetry with respect to electron exchange. For a simplified Hamiltonian described in Eq. (10) and an atom with s^2p^1 , two electrons have the same spin, providing the spin part possesses symmetry in the exchange of these electrons. Thus, the spatial part must be antisymmetric in that exchange. Without loss of generality, the wave function for such an atom in the restricted-space model can be written as [69]

$$\Psi \propto \Psi_{12}(r_1, r_2, r_3) |UUD\rangle + \Psi_{23}(r_1, r_2, r_3) |DUU\rangle + \Psi_{13}(r_1, r_2, r_3) |UDU\rangle.$$
 (13)

Here, U and D represent electrons with spin-up and spin-down, respectively. The subscripts denote the electron pair with respect to exchange of which the wave function is antisymmetric.

The Hamiltonian, Eq. (10), does not affect the spin part of the wave function during evolution. Thus, for simplicity in the numerical implementation, it suffices to evolve only one of the three terms on the right side of Eq. (13). During calculations, we evolve the wave function $\Psi_{12}(r_1, r_2, r_3)$, which is antisymmetric with respect to the exchange of electrons 1 and 2, but neither symmetric nor antisymmetric with respect to the exchange of electrons $1 \leftrightarrow 3$ and $2 \leftrightarrow 3$. The initial wave function, representing the ground state, is obtained using imaginary time propagation of the Hamiltonian, Eq. (10), without the interaction with the field and enforcing the proper symmetry [24].

The numerical solution of the time-dependent Schrödinger equation (TDSE) with the Hamiltonian, Eq. (10), extends the method used in the two-dimensional case described elsewhere [26,36]. The TDSE is solved on a large three-dimensional grid using a split-operator technique and the fast Fourier transform algorithm. For obtaining momentum distributions of outgoing electrons, the wave function cannot be absorbed at the grid's edges. Thus, we divide the evolution space into "bounded motion" and "outer" regions. The evolution in the bounded motion region proceeds without further simplifications, while in the outer regions, the Hamiltonian is successively simplified by neglecting the interaction of electrons with the nucleus and other electrons. This allows representation and evolution of the wave function in the momentum representation in the outer regions, simplifying the evolution to the multiplication by an appropriate phase factor. The transfer between the bounded motion and outer regions is achieved through smooth cutting and coherent adding of the wave function, following the procedure introduced in Ref. [5]. At the simulation's end, the wave function from outer regions can be integrated over the "bounded" part, yielding momentum distributions corresponding to single ionization, double ionization, and triple ionization. The grid has n = 1024 nodes in each direction, with a step size of dr = 0.195. The time step is dt = 0.05, and the total number of steps amounts to 6500. Further details of the algorithm for simulating momentum distributions of the three-electron atom can be found in the Supplemental Material of Ref. [26].

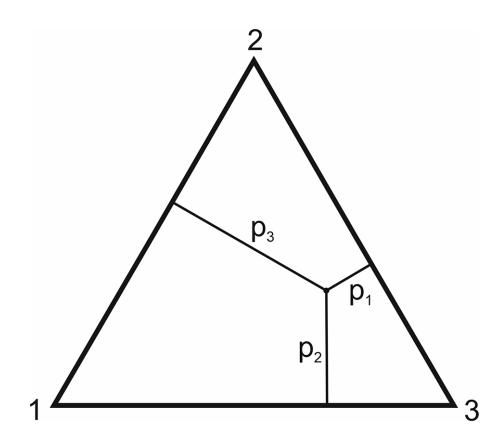


FIG. 1. Schematic visualization of a point in the ternary plot.

C. Dalitz plots

To visualize three-electron distributions we use the socalled Dalitz or ternary plots [26,27,29-31]. These are obtained by first projecting the data onto the sphere of radius $R = (p_1^2 + p_2^2 + p_3^2)^{1/2}$, where p_i is the *i*th electron's momentum along the polarization axis. Then, using gnomonic projection onto planes tangent to the sphere the final ternary plots are reached in each octant of the momentum space. Ternary plots are read in the following way (see Fig. 1): the vertices of the triangle are denoted 1, 2, 3 and correspond to momentum components along the polarization axis of three electrons, i.e., the point of the vertex is equivalent with the statement that the given electron carried all momentum. Positions of the points inside the triangle are defined by a set of three distances p_1 , p_2 , p_3 to the sides of the triangle opposite to vertices 1,2,3, respectively. The closer to the side the point is the smaller momentum is carried by the given electron. In the momentum space spanned by momenta components along the polarization axis there are two types of octants available. The first type are those that collect events in which all electrons propagate in the same hemisphere, i.e., have the same direction of momentum along the polarization axis. In that category there are two octants, marked (+++) or (---). The second type of octants is the one in which one of the electrons has the opposite momentum orientation along the polarization axis relative to the other two electrons, i.e., two electrons propagate in the same hemisphere and the third in the other. In that category there are six octants, marked as (++-) and all possible permutations thereof.

D. Direct vs delayed triple-ionization pathways

In the classical models, we register a triple ionization (TI) event as direct if three electrons ionize shortly after recollision. Namely, we consider the difference between the ionization time of an electron and the time when a recollision takes place. If this time difference is smaller than the time interval when a sharp change occurs in the interelectronic potential energy, we register this electron as ionizing shortly after recollision. Otherwise, if this time difference is larger than the above-defined time interval, we register this electron as ionizing with a delay after recollision. In our studies, we find that the sharp change of the interelectronic potential

energy occurs in a time interval of T/8, with T being the period of the laser field. We register a triple ionization event as delayed if at least one electron ionizes with a delay after recollision. For the intensities considered in this work, we find that the biggest contribution to delayed events is TI events where only one electron ionizes with a delay after recollision. Hence, in what follows, we only consider the latter delayed events and we refer to them as delayed. For TI, we identify direct and delayed events as follows [33,42]:

- (1) We find the ionization time of each of the three electrons, t_{ion}^i .
- (2) We register the maxima in the interelectronic potential energies as a function of time between electron pairs i, j and i, k and j, k during the time intervals when in these pairs one electron is quasifree and the other is bound. Next, for each electron i, we identify the maximum for each one of the i, j and i, k potential energies that is closest to the time $t_{\rm ion}^i$. We denote these times as $t_{\rm rec}^{i,j}$ and $t_{\rm rec}^{i,k}$. We obtain at most six such times for TI events.
- (3) For each time $t_{\text{rec}}^{i,j}$ we identify the time t_2 of closest approach to the core of the quasifree electron (either electron i or j) that is closest to $t_{\text{rec}}^{i,j}$ and denote it as $t_2^{i,j}$. We obtain at most six such times for TI events.

We label an event as direct or delayed TI if four of the times $t_2^{i,j}$ are the same, accounting for one electron being quasifree and the other two bound. That is, if electron i is quasifree during the recollision closest to the ionization time t_{ion}^{i} then the times $t_2^{i,j}$, $t_2^{i,k}$, $t_2^{j,i}$, and $t_2^{k,i}$ should be the same. The times $t_2^{j,i}$ and $t_2^{k,i}$ are associated with the recollision times $t_{\text{rec}}^{j,i}$ and $t_{\text{rec}}^{k,i}$ for the bound electrons j and k, respectively. For the quasifree electron we obtain two recollision times $t_{rec}^{i,j}$ and $t_{rec}^{i,k}$ associated with the ionization time t_{ion}^i . We choose the one with the largest difference from t_{ion}^i , guaranteeing a stricter criterion for direct TI events. Next, we label a TI event as direct if the following conditions are satisfied: $\Delta t_1 = |t_{\rm rec}^{i,j} - t_{\rm ion}^i| < t_{\rm diff}$ or $(t_{\rm ion}^i < t_{\rm rec}^{i,j})$ and $t_{\rm ion}^i < t_{\rm rec}^{i,k}$ and $t_{\rm ion}^i < t_{\rm rec}^{i,k}$ and $t_{\rm ion}^i < t_{\rm rec}^{i,j}$ and $t_{\rm ion}^i < t_{\rm ion}^i| < t_{\rm diff}$ and $t_{\rm ion}^i < t_{\rm ion}^i| < t_{\rm diff}$. The condition $(t_{\rm ion}^i < t_{\rm rec}^{i,j})$ and $t_{\rm ion}^i < t_{\rm ion}^i| < t_{\rm ion}^i|$ $t_{\rm rec}^{i,k}$) has also been used in our previous studies [14,70] to account for a quasifree electron ionizing significantly earlier before recollision. This happens mostly at high intensities. We label events as delayed pathway TI, when two electrons ionize shortly after recollision, while one electron ionizes with a delay. That is, for these delayed events one out of the three times Δt_1 , Δt_2 , and Δt_3 is larger than t_{diff} and the other two times are less than t_{diff} . The time t_{diff} is determined by the time interval where the interelectronic potential energy undergoes a sharp change due to a recollision. For the intensities considered here, we find $t_{\rm diff} \approx T/8$.

III. RESULTS AND DISCUSSIONS

A. Laser pulse parameters for the semiclassical and quantum models

For the Ne results presented in this work, for the ECBB and H models we consider a pulse duration of $\tau = 25$ fs, wavelength of 800 nm and intensities 1, 1.3, and 1.6 PW/cm². For the quantum model, the pulse duration is three optical cycles with wavelength 760 nm and intensities 0.5, 0.75, 1.7,

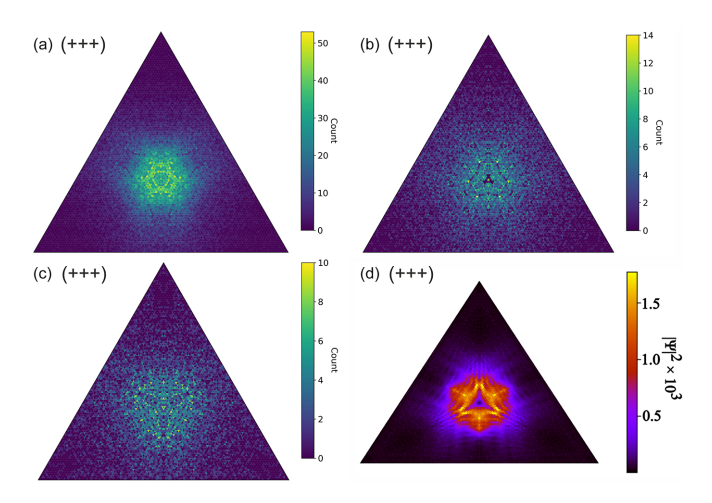


FIG. 2. Momenta distributions for triple ionization events visualized with the help of Dalitz plots (ternary plots): (a) semiclassical calculations with the ECBB model, $I=1.6~\mathrm{PW/cm^2}$; (b) semiclassical calculations with the H model, $\alpha=2$, $I=1.6~\mathrm{PW/cm^2}$; (c) semiclassical calculations with the H model, $\alpha=4$, $I=1.6~\mathrm{PW/cm^2}$; (d) quantum calculations, $I=1.7~\mathrm{PW/cm^2}$.

and 2.55 PW/cm². We have used these parameters in previous semiclassical [42] as well as quantum studies [24–26,67–69] addressing triple ionization in strongly driven Ne. Another reason we use the same parameters as in previous studies for the semiclassical and quantum models is that these are extremely demanding computations. Also, the focus of this work is not a quantitative comparison of the two models but rather a qualitative one that focuses on interpreting the features of the Dalitz plots and attributing them to different ionization pathways. In this sense, having different parameters for the semiclassical and quantum models allows us to cover a wider parameter space, see, for instance, Fig. 4(e). Finally, to ensure that where we directly compare the distributions obtained with the ECBB model and the quantum model, see Fig. 2, our results and conclusions are not affected by the difference in the laser parameters, we have performed a computation with the ECBB model for a wavelength of 760 nm and an intensity of 1.7 PW/cm², i.e., the parameters of the quantum model. We find almost identical results with those presented in this work for the ECBB model for a wavelength of 800 nm and intensity of 1.6 PW/cm². Moreover, we note that we consider a longer pulse duration for the semiclassical models, since otherwise the results would be phase dependent and significantly more computationally challenging to obtain. However, we expect that a shorter pulse duration would result in an even bigger contribution of the direct pathway in the ECBB model and hence a more pronounced central "spot" (see discussion below) and an even better agreement with quantum results.

B. General observations

Let us begin our discussion by presenting the main features of correlated triple ionization on Dalitz plots, see Fig. 2. Figures 2(a)–2(c) correspond to results obtained with the two semiclassical models and Fig. 2(d) to results obtained with the quantum model. For the distribution presented in Fig. 2(a) we used the ECBB model, whereas for Figs. 2(b) and 2(c) we

used the H model with different values of the parameter α ; for the quantum case the soft-core 1D+1D+1D potential is used. We find that for each of the plots in Fig. 2 the momentum distribution is concentrated and peaked in the middle of the triangle and stretches towards its sides. The interpretation of the observed distribution is rather straightforward. The peak in the middle of the triangle corresponds to dominance, for the chosen laser intensity, of events in which all three electrons escape in the same hemisphere, i.e., the electrons are escaping in the same direction along the polarization of the laser field, with similar momenta. The tails of the distribution that stretch towards the sides of the triangle correspond to events in which one of the three electrons has significantly smaller momentum compared with the other two electrons, which escape with similar momenta.

While the final state of the escaping electrons is easily read from the distributions in Fig. 2, the pathway that leads to this state is not immediately evident. We attribute features of these distributions to different pathways the electrons follow to escape by further analyzing the results obtained with the semiclassical ECBB model. In Fig. 3, we present the Dalitz plots according to the triple ionization pathway the electrons follow to escape. Figures 3(a) and 3(b) (top row) show all TI events, Figs. 3(e) and 3(f) (bottom row) show direct TI events, where all electrons escape simultaneously after recollision. Also, Figs. 3(c) and 3(d) (middle row) show delayed TI events, where two electrons escape immediately after recollision and one escapes with a delay. For the intensities considered when using the ECBB model, the direct and delayed pathways contribute roughly equally and account for more than 85% of all events. Also, Figs. 3(a), 3(c), and 3(e) (left column) show TI events where electrons escape in the same direction along the laser polarization axis, whereas Figs. 3(b), 3(d), and 3(f) (right column) show TI events where one of the three electrons escapes in a direction opposite to the other two electrons. Comparing the different rows in Fig. 3, it is clear that the direct TI events predominantly populate the center of the momentum distribution, while delayed events populate the tails. In addition, inspection of the right column in Fig. 3 reveals that the electron escaping in the opposite direction does so with much lower momentum compared with the other two electrons escaping with similar momenta. What is more, such events correspond mostly to delayed ionization. In view of the above associations between features of the Dalitz plots and TI pathways, Fig. 4 reveals that for the ECBB model direct ionization becomes more dominant with increasing intensity from 1 to 1.6 PW/cm² [see Figs. 4(f)-4(h)]. A similar trend is observed for the quantum-mechanical calculations with increasing intensity from 0.5 to 1.7 PW/cm² [see Figs. 4(a)-4(d)]. In the following, we refer to the part of the momentum distribution located in the middle of the triangle that corresponds to the direct ionization as the central spot.

Results obtained with the quantum model need some further commenting. In Figs. 4(a)–4(d) we show momenta distributions for triple ionization events in which all electrons escape in the same direction with respect to the laser polarization axis. First, the model we use was designed to trace direct ionization by restriction of the space to specified tracks along which electrons may move. These tracks were

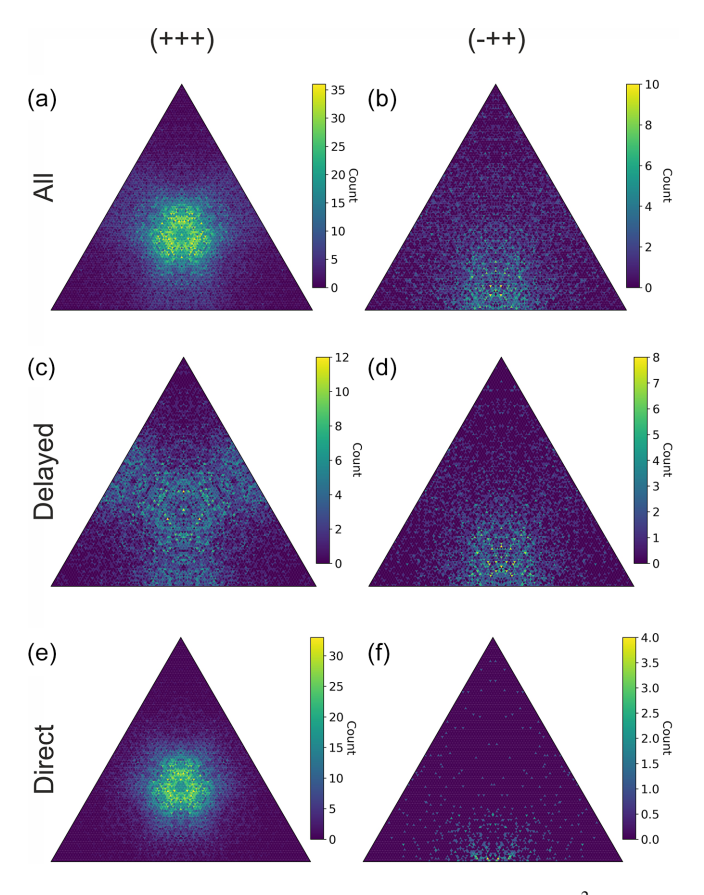


FIG. 3. Dalitz plots for TI events at $I = 1.3 \text{ PW/cm}^2$ obtained with the ECBB model: Panels (a) and (b) show all events, panels (c) and (d) show delayed ionization events, and panels (e) and (f) show direct ionization events. For panels (a), (c), and (e), ternary plots are obtained for all electrons moving in one direction. For panels (b), (d), and (f), ternary plots are obtained for one electron escaping in a direction opposite with respect to the other two electrons (bottom corners of triangle correspond to electrons moving in the same direction). For all panels the classical events were symmetrized to account for the electrons being indistinguishable.

chosen to coincide with lines along which classical saddle points of potential move when the field intensity is changed (see discussion on saddles in Refs. [7,65] and its application in Refs. [24,36,71]). Such a choice of track favors direct ionization making it more visible, while keeping overall very good agreement with experiments [47]. Second, the quantum calculations are performed for very short pulses ($n_c = 3$) and for single CEP ($\phi = 0$). Thus, concerning comparison with semiclassical results, one may only compare overall trends, since the quantum momenta distributions are phase-dependent [72] due to the short laser-pulses employed. Moreover, in the quantum case, disentangling the three-electron momenta distribution into parts that correspond to the direct and delayed paths of ionization, in a similar way as is done for semiclassical results (see Fig. 3), is beyond capabilities offered by our approach. Since all ionization paths, possible in our model, give their input to the final distribution of electron momenta, the observed complex pattern is a consequence of their relative contribution. However, the quantum and semiclassical (mainly the ECBB model) Dalitz plots resemble each

other. Indeed, they both have the central spot that does not change its width significantly as the field intensity changes [see Fig. 4(e)]. Thus one can argue that the direct ionization channel indeed may be contained within the quantum Dalitz (+++) plots, and even dominate the distributions there for all studied intensities except the highest one. For the intensity $I = 2.55 \text{ PW/cm}^2$, Fig. 4(d), three separate maxima located at some distance from the center of the triangle are visible, suggesting stronger contribution of delayed ionization. The resemblance between Figs. 4(c) and 4(h), i.e., between the quantum and the semiclassical Dalitz plots, is striking.

An interesting conclusion can be made about the role of soft-core potentials in strong-field simulations. Soft-core potentials are very useful and often are the first-choice tools for simulations, both in classical and quantum realms. As an example, we recall the work by Majorosi, Benedict, and Czirják [73], where HHG obtained with a 3D hydrogen model including the Coulomb potential was successfully reproduced with a single-dimensional soft-core potential model. However, the first choice is not necessarily the finest one. The Heisenberg potential (H model) effectively leads to softening of the Coulomb singularity [33,42], therefore in the following discussion the H model will serve as an example of a soft-core semiclassical model. At first glance, the general shapes of momentum distributions obtained by both H model and ECBB are similar, and one is tempted to assume that the particular choice of potentials for simulations should not change the qualitative picture of triple ionization. Nevertheless, a more careful analysis of Fig. 2 reveals that correlated escapes are less prominent in Figs. 2(b) and 2(c), than in Fig. 2(a). When these results are compared with the quantum results in Fig. 2(d), it is justified to conclude that the ECBB model is better suited for tracing correlations during multi-electron escape. Let us recall that the quantum model considered here is designed in a way that favors the direct (correlated) escape despite the fact that it uses the soft-core potential. Whether there are better potentials in the case of simplified quantum models remains an open issue.

C. The central spot in Dalitz plots

The correspondence of the central spot in Dalitz (+ + +)plots mainly with the direct triple ionization channel has been discussed in the previous section. That discussion can be culminated to four important conclusions or conjectures: (i) the spot in semiclassical (+++) Dalitz plots is unambiguously connected with direct triple ionization; (ii) semiclassical and quantum (+++) Dalitz plots are quite similar; (iii) it is possible to argue for a general correspondence between semiclassical and quantum notions of direct ionization, and (iv) the size of the spot is nearly independent for a wide interval of field intensities for both quantum and semiclassical models. Since the central spot is formed predominantly by the direct channel, then a simplified classical model for direct triple ionization is expected to reproduce especially the last property. In what follows, we construct such a simple classical model for direct triple ionization events and show that this model indeed predicts a nearly constant size of a spot in Dalitz (+++) plots. Recalling the three-step model, initially one electron tunnel-ionizes close to the field maximum. Then, it

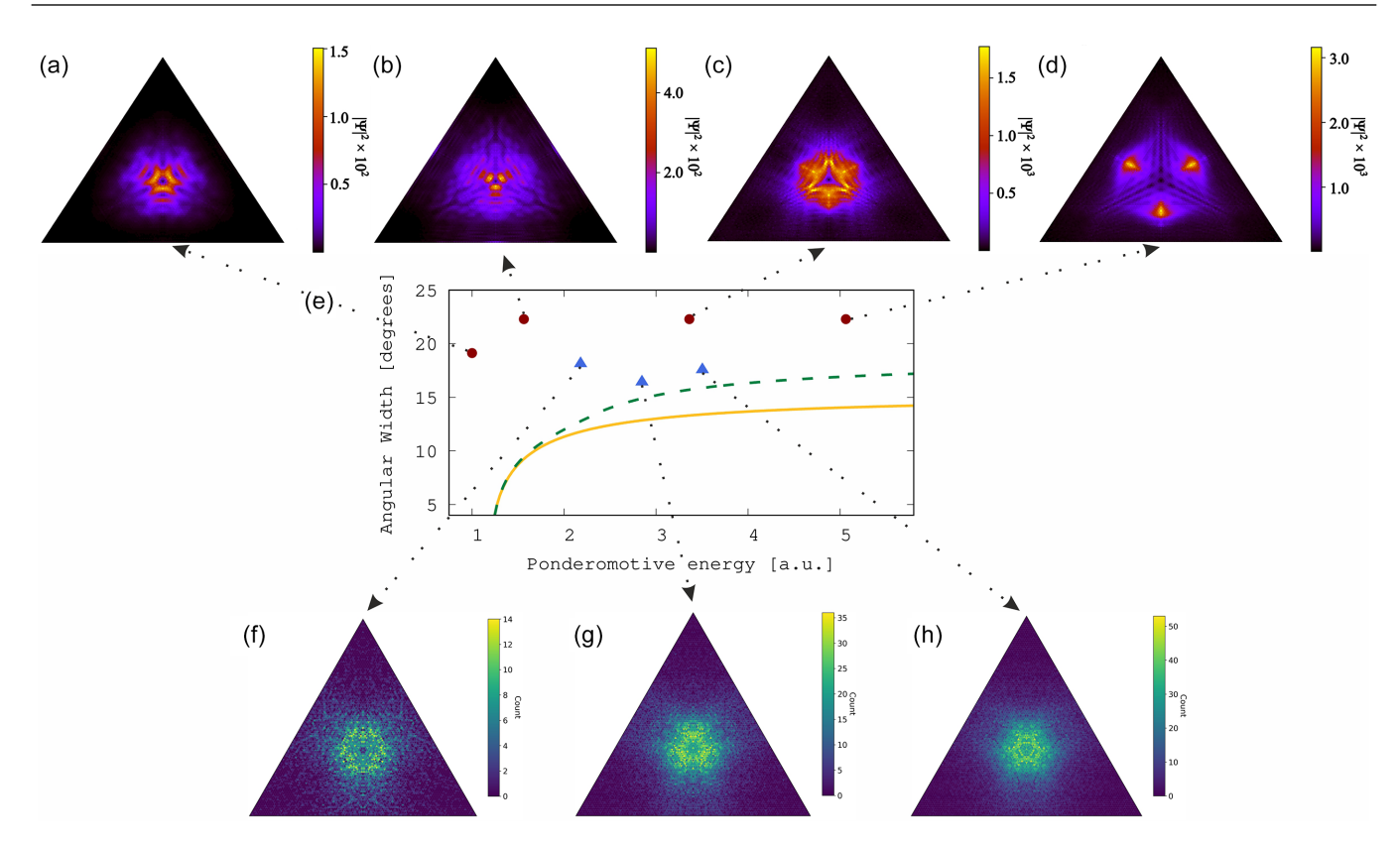


FIG. 4. Dalitz plots for data from quantum calculations: (a) $I = 0.5 \text{ PW/cm}^2$, (b) $I = 0.75 \text{ PW/cm}^2$, (c) $I = 1.7 \text{ PW/cm}^2$, (d) $I = 2.55 \text{ PW/cm}^2$. (e) Dependence of the angular half-width of three-electron momentum distribution in (+ + +) octant after direct triple ionization on the value of the ponderomotive energy of the electron gained by the laser field—the quantum-mechanical model (circles), the classical model (triangles) and simplified analytic models (solid line β_{3E}^s , dashed line β_{3E})—see discussion in the text. Dalitz plots for data from ECBB semiclassical calculations: (f) $I = 1 \text{ PW/cm}^2$, (g) $I = 1.3 \text{ PW/cm}^2$, and (h) $I = 1.6 \text{ PW/cm}^2$.

propagates in the field and can turn back and recollide with its parent ion. Upon recollision, the energy gained by the electron in the laser field minus the energy spent to overcome the ionization potential is redistributed among all three electrons, i.e., among the tunnel-ionizing and the two bound electrons. In a direct triple ionization event, the electrons are released soon after recollision. Also, we consider that triple ionization takes place following just one recollision, which is supported by our semiclassical calculations [42]. In this simplified classical model, we ignore the Coulomb potential and any electron-electron interaction. Hence, as a result of a single recollision in a direct triple ionization event, an electron can gain a momentum p_0 due to the energy redistributed by the tunnel-ionizing electron upon recollision. However, an electron also gains an additional momentum Δp —a boost from the electric field of the laser pulse, which is equal to minus the value of the vector potential at the time of ionization, similar to attosecond streaking [74]. In this simplified model, the momentum shift Δp of each electron is the same, thus, in the case when all electrons escape in the same direction, for instance (+++), the final momentum distribution is simply shifted from p_0 .

It is easiest to first illustrate the above ideas for double ionization, see Fig. 5. If the energy of the returning electron is U_r and the ionization potential of the bound electron is I_{p2} (second ionization potential), then the total energy that is shared among the two electrons just after recollision is $U_r - I_{p2}$. For

a monochromatic laser field, the maximum total energy is $E_{tm} = 3.17U_p - I_{p2}$. Also, the additional momentum Δp is given by $\pm 2\xi \sqrt{U_p}$, where ξ accounts for the recollision time shift with respect to the time when the vector potential has its maximum [75]. For the case of an electron returning to the ion

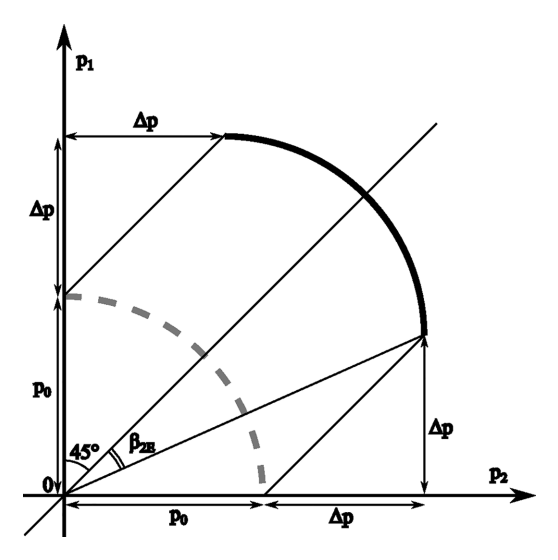


FIG. 5. Schematic illustration of the momentum distribution that electrons gain upon a single recollision in the laser field. See text for explanation of values depicted here.

with the maximum possible energy, i.e., $3.17U_p$, one obtains approximately $\xi \approx 0.95$. Hence, in the momentum space, any direct double-ionization event is placed in the right-upper quarter (or left-bottom) of the circle $p_1^2 + p_2^2 = 2E_{tm}$, see gray-dashed line in Fig. 5. Results are similar for both quarters so we only focus on the right-upper one, see Fig. 5. The radius of the circle is $p_0 = \sqrt{2E_{tm}}$. Following ionization, the laser field is shifting the electron momentum by $\Delta p = 2\xi\sqrt{U_p}$, giving rise to the black-solid line in Fig. 5. It is clear from the geometry in Fig. 5 that the angle between the diagonal and one of the black-solid-line endpoints is equal to

$$\beta_{2E} = \frac{\pi}{4} - \arctan \frac{\Delta p}{\Delta p + p_0}$$

$$= \frac{\pi}{4} - \arctan \frac{2\xi\sqrt{U_p}}{2\xi\sqrt{U_p} + \sqrt{2(3.17U_p - I_{p2})}}.$$
 (14)

This angle corresponds to the maximum deviation from the diagonal where both electrons have the same momentum. Hence, for double ionization the distribution of direct ionization events will be within the angle $2\beta_{2E}$ from Eq. (14).

Following a similar reasoning, we next obtain the corresponding angle β for direct triple-ionization events. Direct events are placed in the (+++) and (---) octants of a sphere in momentum space. We illustrate our ideas focusing on the octant (+++). In this case, the angle β_{3E}^s , where s stands for "simplified," is obtained in a similar manner as β_{2E} —the difference being that the angle $\arctan(\Delta p/[\sqrt{2}\Delta p + p_0])$ is not subtracted from $\pi/4$ but from the angle between the main diagonal of the octant and its bottom plane, which is $\arctan(\sqrt{2}/2)$. Also, the momentum p_0 is determined in a similar way as for two electrons, i.e., $p_0 = \sqrt{2(3.17U_p - I_{p23})}$, where I_{p23} stands for the sum of the second and third ionization potentials. For Ne considered here $I_{p23} = 3.83$ a.u. Thus, we obtain

$$\beta_{3E}^{s} = \arctan\left(\frac{\sqrt{2}}{2}\right) - \arctan\frac{1.9\sqrt{U_p}}{1.9\sqrt{2U_p} + \sqrt{2(3.17U_p - I_{p23})}}.$$
 (15)

In Fig. 4(e) the solid yellow line shows the dependence of the angle β_{3E}^s on U_p . Although the curve does not fit the exact values of the angle extracted from our simulations, it shows the same trend; that is, first the angle grows and then it saturates.

In the model discussed above, we assumed that the rescattering electron (i) starts its one-dimensional motion along the field-polarization direction at the position of the atomic core and (ii) propagates in the external electric field, while Coulomb interactions with all other particles are ignored until the rescattering electron returns to the core. At this instant, the rescattering electron can instantly redistribute its energy between itself and the two other electrons that have a total bound energy of I_{23} . In this model, we also assume that the rescattering electron (iii) starts its motion at a time such that this electron returns to the core with the maximum energy $3.17U_p$; this time may be interpreted as the tunnel-ionization time through the field-lowered Coulomb potential (which cor-

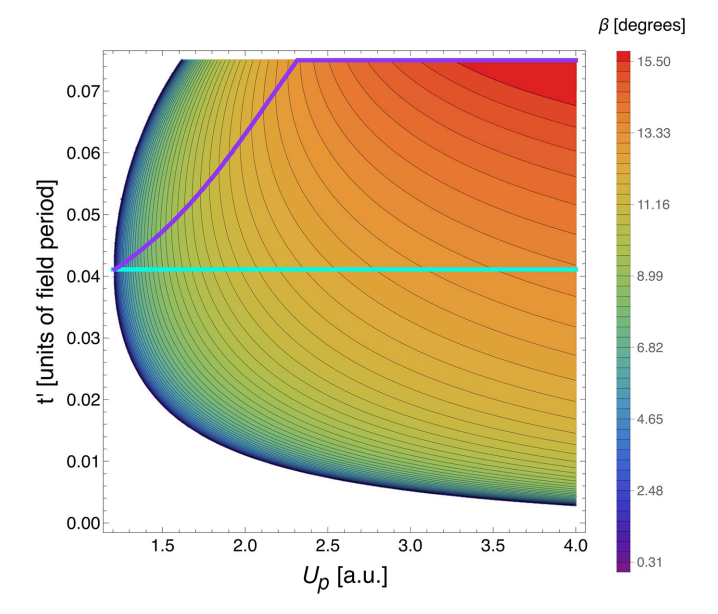


FIG. 6. Angle β_{3E}^M dependence on the time of tunnel ionization of the rescattering electron and on the ponderomotive energy. The purple curve identifies the value of the tunnel-ionization time t' that corresponds to the largest possible β_{3E}^M for each U_p . The turquoise curve identifies the angle $\beta_{3E}^M = \beta_{3E}^s$ that corresponds to the time t' that results in $\xi = 0.95$ and $\kappa = 3.17$.

responds to the start of the propagation time in the ECBB model).

Next, we introduce an improvement to assumption (iii) of this simplified model. We allow the rescattering electron to tunnel-ionize at different times t', which can lead to the electron returning to the core with energy smaller than $3.17U_p$ but potentially with larger angles β_{3E} . In this modified model, both the momentum $2\xi(t')\sqrt{U_p}$ and the energy $\kappa(t')U_p$ of the rescattering electron upon its return to the core depend on the time t', with $\kappa=3.17$ corresponding to the maximum return energy. The formula for β_{3E}^M , with M standing for "modified," takes the form

$$\beta_{3E}^{M} = \arctan\left(\frac{\sqrt{2}}{2}\right)$$

$$-\arctan\frac{2\xi(t')\sqrt{U_p}}{2\xi(t')\sqrt{2U_p} + \sqrt{2(\kappa(t')U_p - I_{p23})}}. \quad (16)$$

In Fig. 6, we show the dependence of the angle β_{3E}^M on both U_p and t'. We note that the time t' in Fig. 6 changes from the time corresponding to the maximum of the electric field plus to this time and a time interval such that the ionization rate is not very low. We find that, for each value of U_p there exists a time t' that maximizes β_{3E}^M . This one-to-one dependence is represented with the purple curve in Fig. 6. The turquoise curve identifies the angle $\beta_{3E}^M = \beta_{3E}^s$ that corresponds to the time t' that results in $\kappa = 3.17$. We find that the improved simplified model results in an angle $\beta_{3E}^M > \beta_{3E}^s$. This is better illustrated as a function of U_p in Fig. 4(e), where $\beta_{3E}^M(U_p)$ is depicted with a dashed-green line, while $\beta_{3E}^s(U_p)$ corresponding to the maximum return energy of 3.17 U_p is depicted with a solid yellow line. We also find

that in Fig. 4(e) the angle $\beta_{3E}^M(U_p)$ agrees better than $\beta_{3E}^s(U_p)$ with the results obtained from the ECBB model depicted with the blue triangles. This is expected since the variation of the tunnel-ionization time t' is naturally embedded in the ECBB model.

Next, we discuss the behavior of the angles $\beta_{3E}^{M/s}(U_p)$ in Fig. 4(e) for lower field intensities. The simplified classical model provides angles $\beta_{3E}^{M/s}(U_p)$, i.e., the width of the central spot, only for ponderomotive energies larger than $I_{p_{23}}/3.17$, see Eqs. (15) and (16). We also find that, for low intensities, $\beta_{3E}^{M/s}(U_p)$ differ significantly from the corresponding values obtained with the quantum and the ECBB model. The main reason is that, in the simplified model we do not account for Coulomb interactions.

Also, the quantum and classical results in Fig. 4(e) reflect the same trend, i.e., a nearly constant width of the momentum distribution when the intensity increases. However, unsurprisingly, the measured values of β obtained from quantum simulations do not fit as well as the ECBB classical model the results obtained with our simplified classical model. The quantum calculations are performed using a reduced-dimensionality model; therefore, one can only expect qualitative agreement with the simplified classical model. This trend of a nearly constant width of the momentum distribution as a function of intensity is also reproduced by the simplified classical model. Indeed, a comparison of $\beta_{3E}^M(U_p)$ with $\beta_{3F}^{s}(U_p)$ suggests that the width of the momentum distribution mainly depends on the tunnel-ionization time (simplified model) and subsequently on the time of recollision and hence does not change significantly with the intensity of the field. Both curves saturate for large values of U_p . The remaining discrepancies of the simplified model with the quantum model and the ECBB model most probably stem from not accounting for electron-electron and electron-ion interactions in the simplified model. Hence, the simplified model reproduces the main features of the angle β_{3E} as a function of U_p .

IV. CONCLUSIONS

We have provided an analysis of signatures of particular triple ionization channels in Dalitz plots of the electron momenta. We have compared data obtained after simulations with a quantum-mechanical restricted-space model with data obtained with semiclassical simulations with the ECBB and Heisenberg models. After a qualitative comparison of the corresponding Dalitz plots, we find that the results for all numerical models suggest that a central spot in Dalitz plots for electrons propagating all in the same hemisphere correspond to direct ionization. We have rationalized our hypothesis, constructing a simple classical model for direct ionization that predicts how the spot size changes with increasing intensity of the laser field. The model independence of this imprint of direct ionization manifested on Dalitz plots, suggests that the occurrence of this central spot in Dalitz plots should also be observed in experiments.

ACKNOWLEDGMENTS

We gratefully acknowledge the Polish high-performance computing infrastructure PLGrid (HPC Center: ACK Cyfronet AGH) for providing computer facilities and support within Computational Grant No. PLG/2024/017146. This work was realized under National Science Centre (Poland) project Symfonia No. 2016/20/W/ST4/00314. J.S.P.-B. would like to thank Michal Ojczenasz for help in preparing the script for obtaining ternary plots.

- [1] R. Borrego-Varillas, M. Lucchini, and M. Nisoli, Attosecond spectroscopy for the investigation of ultrafast dynamics in atomic, molecular and solid-state physics, Rep. Prog. Phys. 85, 066401 (2022).
- [2] P. B. Corkum, Plasma perspective on strong field multiphoton ionization, Phys. Rev. Lett. **71**, 1994 (1993).
- [3] B. Walker, B. Sheehy, L. F. DiMauro, P. Agostini, K. J. Schafer, and K. C. Kulander, Precision measurement of strong field double ionization of helium, Phys. Rev. Lett. 73, 1227 (1994).
- [4] J. B. Watson, A. Sanpera, D. G. Lappas, P. L. Knight, and K. Burnett, Nonsequential double ionization of helium, Phys. Rev. Lett. 78, 1884 (1997).
- [5] M. Lein, E. K. U. Gross, and V. Engel, Intense-field double ionization of helium: Identifying the mechanism, Phys. Rev. Lett. 85, 4707 (2000).
- [6] J. S. Parker, D. H. Glass, L. R. Moore, E. S. Smyth, K. T. Taylor, and P. G. Burke, Time-dependent and time-independent methods applied to multiphoton ionization of helium, J. Phys. B: At., Mol. Opt. Phys. 33, L239 (2000).
- [7] K. Sacha and B. Eckhardt, Pathways to double ionization of atoms in strong fields, Phys. Rev. A 63, 043414 (2001).
- [8] J. S. Parker, B. J. S. Doherty, K. T. Taylor, K. D. Schultz, C. I. Blaga, and L. F. DiMauro, High-energy cutoff in the spectrum

- of strong-field nonsequential double ionization, Phys. Rev. Lett. **96**, 133001 (2006).
- [9] A. Staudte, C. Ruiz, M. Schöffler, S. Schössler, D. Zeidler, Th. Weber, M. Meckel, D. M. Villeneuve, P. B. Corkum, A. Becker, and R. Dörner, Binary and recoil collisions in strong field double ionization of helium, Phys. Rev. Lett. 99, 263002 (2007).
- [10] A. Rudenko, V. L. B. de Jesus, Th. Ergler, K. Zrost, B. Feuerstein, C. D. Schröter, R. Moshammer, and J. Ullrich, Correlated two-electron momentum spectra for strong-field nonsequential double ionization of He at 800 nm, Phys. Rev. Lett. 99, 263003 (2007).
- [11] C. Figueira de Morisson Faria and X. Liu, Electron–electron correlation in strong laser fields, J. Mod. Opt. **58**, 1076 (2011).
- [12] W. Becker, X.-J. Liu, P. J. Ho, and J. H. Eberly, Theories of photoelectron correlation in laser-driven multiple atomic ionization, Rev. Mod. Phys. 84, 1011 (2012).
- [13] B. Bergues, M. Kübel, N. G. Johnson, B. Fischer, N. Camus, K. J. Betsch, O. Herrwerth, A. Senftleben, A. M. Sayler, T. Rathje, T. Pfeifer, I. Ben-Itzhak, R. R. Jones, G. G. Paulus, F. Krausz, R. Moshammer, J. Ullrich, and M. F. Kling, Attosecond tracing of correlated electron-emission in non-sequential double ionization, Nat. Commun. 3, 813 (2012).

- [14] G. P. Katsoulis, A. Hadjipittas, B. Bergues, M. F. Kling, and A. Emmanouilidou, Slingshot nonsequential double ionization as a gate to anticorrelated two-electron escape, Phys. Rev. Lett. 121, 263203 (2018).
- [15] A. Rudenko, K. Zrost, B. Feuerstein, V. L. B. de Jesus, C. D. Schröter, R. Moshammer, and J. Ullrich, Correlated multielectron dynamics in ultrafast laser pulse interactions with atoms, Phys. Rev. Lett. 93, 253001 (2004).
- [16] K. Zrost, A. Rudenko, Th. Ergler, B. Feuerstein, V. L. B. de Jesus, C. D. Schröter, R. Moshammer, and J. Ullrich, Multiple ionization of Ne and Ar by intense 25 fs laser pulses: Fewelectron dynamics studied with ion momentum spectroscopy, J. Phys. B: At., Mol. Opt. Phys. 39, S371 (2006).
- [17] A. Rudenko, Th. Ergler, K. Zrost, B. Feuerstein, V. L. B. de Jesus, C. D. Schröter, R. Moshammer, and J. Ullrich, From non-sequential to sequential strong-field multiple ionization: Identification of pure and mixed reaction channels, J. Phys. B: At., Mol. Opt. Phys. 41, 081006 (2008).
- [18] O. Herrwerth, A. Rudenko, M. Kremer, V. L. B. de Jesus, B. Fischer, G. Gademann, K. Simeonidis, A. Achtelik, Th. Ergler, B. Feuerstein, C. D. Schröter, R. Moshammer, and J. Ullrich, Wavelength dependence of sub-laser-cycle few-electron dynamics in strong-field multiple ionization, New J. Phys. 10, 025007 (2008).
- [19] K. Sacha and B. Eckhardt, Nonsequential triple ionization in strong fields, Phys. Rev. A **64**, 053401 (2001).
- [20] C. Ruiz, L. Plaja, and L. Roso, Lithium ionization by a strong laser field, Phys. Rev. Lett. 94, 063002 (2005).
- [21] P. J. Ho and J. H. Eberly, In-plane theory of nonsequential triple ionization, Phys. Rev. Lett. 97, 083001 (2006).
- [22] P. J. Ho and J. H. Eberly, Argon-like three-electron trajectories in intense-field double and triple ionization, Opt. Express 15, 1845 (2007).
- [23] J. Guo and X.-S. Liu, Lithium ionization by an intense laser field using classical ensemble simulation, Phys. Rev. A 78, 013401 (2008).
- [24] J. H. Thiede, B. Eckhardt, D. K. Efimov, J. S. Prauzner-Bechcicki, and J. Zakrzewski, *Ab initio* study of time-dependent dynamics in strong-field triple ionization, Phys. Rev. A 98, 031401(R) (2018).
- [25] J. S. Prauzner-Bechcicki, D. K. Efimov, M. Mandrysz, and J. Zakrzewski, Strong-field triple ionisation of atoms with p^3 valence shell, J. Phys. B: At., Mol. Opt. Phys. **54**, 114001 (2021).
- [26] D. K. Efimov, A. Maksymov, M. Ciappina, J. S. Prauzner-Bechcicki, M. Lewenstein, and J. Zakrzewski, Three-electron correlations in strong laser field ionization, Opt. Express 29, 26526 (2021).
- [27] H. Jiang, D. Efimov, F. He, and J. S. Prauzner-Bechcicki, Dalitz plots as a tool to resolve nonsequential paths in strong-field triple ionization, Phys. Rev. A **105**, 053119 (2022).
- [28] A. Emmanouilidou, Recoil collisions as a portal to field-assisted ionization at near-UV frequencies in the strong-field double ionization of helium, Phys. Rev. A 78, 023411 (2008).
- [29] M. Schulz, R. Moshammer, W. Schmitt, H. Kollmus, R. Mann, S. Hagmann, R. E. Olson, and J. Ullrich, Correlated threeelectron continuum states in triple ionization by fast heavy-ion impact, Phys. Rev. A 61, 022703 (2000).
- [30] M. F. Ciappina, W. R. Cravero, M. Schulz, R. Moshammer, and J. Ullrich, Theoretical description of two- and three-particle

- interactions in single ionization of helium by ion impact, Phys. Rev. A **74**, 042702 (2006).
- [31] M. Schulz, D. Fischer, T. Ferger, R. Moshammer, and J. Ullrich, Four-particle Dalitz plots to visualize atomic break-up processes, J. Phys. B: At., Mol. Opt. Phys. 40, 3091 (2007).
- [32] K. Amini, J. Biegert, F. Calegari, A. Chacón, M. F. Ciappina, A. Dauphin, D. K. Efimov, C. Figueira de Morisson Faria, K. Giergiel, P. Gniewek, A. S. Landsman, M. Lesiuk, M. Mandrysz, A. S. Maxwell, R. Moszyński, L. Ortmann, J. Antonio Pérez-Hernández, A. Picón, E. Pisanty, J. Prauzner-Bechcicki, K. Sacha, N. Suárez, A. Zaïr, J. Zakrzewski, and M. Lewenstein, Symphony on strong field approximation, Rep. Prog. Phys. 82, 116001 (2019).
- [33] M. B. Peters, G. P. Katsoulis, and A. Emmanouilidou, General model and toolkit for the ionization of three or more electrons in strongly driven atoms using an effective Coulomb potential for the interaction between bound electrons, Phys. Rev. A 105, 043102 (2022).
- [34] J. S. Parker, E. S. Smyth, and K. T. Taylor, Intense-field multiphoton ionization of helium, J. Phys. B: At., Mol. Opt. Phys. **31**, L571 (1998).
- [35] C. Ruiz, L. Plaja, L. Roso, and A. Becker, *Ab initio* calculation of the double ionization of helium in a few-cycle laser pulse beyond the one-dimensional approximation, Phys. Rev. Lett. 96, 053001 (2006).
- [36] J. S. Prauzner-Bechcicki, K. Sacha, B. Eckhardt, and J. Zakrzewski, Quantum model for double ionization of atoms in strong laser fields, Phys. Rev. A 78, 013419 (2008).
- [37] L. D. Landau and E. M. Lifshitz, *Quantum Mechanics: Non-Relativistic Theory*, 2nd ed. (Pergamon, Oxford, 1965).
- [38] N. B. Delone and V. P. Krainov, Energy and angular electron spectra for the tunnel ionization of atoms by strong low-frequency radiation, J. Opt. Soc. Am. B 8, 1207 (1991).
- [39] S. L. Haan, R. Grobe, and J. H. Eberly, Numerical study of autoionizing states in completely correlated two-electron systems, Phys. Rev. A **50**, 378 (1994).
- [40] C. L. Kirschbaum and L. Wilets, Classical many-body model for atomic collisions incorporating the Heisenberg and Pauli principles, Phys. Rev. A 21, 834 (1980).
- [41] J. S. Cohen, Quasiclassical effective Hamiltonian structure of atoms with z=1 to 38, Phys. Rev. A **51**, 266 (1995).
- [42] A. Emmanouilidou, M. B. Peters, and G. P. Katsoulis, Singularity in the electron-core potential as a gateway to accurate multielectron ionization spectra in strongly driven atoms, Phys. Rev. A 107, L041101 (2023).
- [43] R. R. Pandit, V. R. Becker, K. Barrington, J. Thurston, L. Ramunno, and E. Ackad, Comparison of the effect of soft-core potentials and Coulombic potentials on bremsstrahlung during laser matter interaction, Phys. Plasmas 25, 043302 (2018).
- [44] R. R. Pandit, Y. Sentoku, V. R. Becker, K. Barrington, J. Thurston, J. Cheatham, L. Ramunno, and E. Ackad, Effect of soft-core potentials on inverse bremsstrahlung heating during laser matter interactions, Phys. Plasmas 24, 073303 (2017).
- [45] J. Feist, S. Nagele, R. Pazourek, E. Persson, B. I. Schneider, L. A. Collins, and J. Burgdörfer, Nonsequential two-photon double ionization of helium, Phys. Rev. A 77, 043420 (2008).
- [46] X.-L. Hao, J. Chen, W.-D. Li, B. Wang, X. Wang, and W. Becker, Quantum effects in double ionization of argon below the threshold intensity, Phys. Rev. Lett. **112**, 073002 (2014).

- [47] D. K. Efimov, A. Maksymov, J. S. Prauzner-Bechcicki, J. H. Thiede, B. Eckhardt, A. Chacón, M. Lewenstein, and J. Zakrzewski, Restricted-space *ab initio* models for double ionization by strong laser pulses, Phys. Rev. A 98, 013405 (2018).
- [48] G. Basnayake, S. Fernando, S. K. Lee, D. A. Debrah, G. A. Stewart, and W. Li, The lack of electron momentum correlation in strong-field triple ionisation of molecules, Mol. Phys. 120, e1931722 (2022).
- [49] S. Grundmann, V. V. Serov, F. Trinter, K. Fehre, N. Strenger, A. Pier, M. Kircher, D. Trabert, M. Weller, J. Rist, L. Kaiser, A. W. Bray, L. Ph. H. Schmidt, J. B. Williams, T. Jahnke, R. Dörner, M. S. Schöffler, and A. S. Kheifets, Revealing the two-electron cusp in the ground states of He and H₂ via quasifree double photoionization, Phys. Rev. Res. 2, 033080 (2020).
- [50] S. Larimian, S. Erattupuzha, A. Baltuška, M. Kitzler-Zeiler, and X. Xie, Frustrated double ionization of argon atoms in strong laser fields, Phys. Rev. Res. 2, 013021 (2020).
- [51] S. Mikaelsson, J. Vogelsang, C. Guo, I. Sytcevich, A.-L. Viotti, F. Langer, Y.-C. Cheng, S. Nandi, W. Jin, A. Olofsson, R. Weissenbilder, J. Mauritsson, A. L'Huillier, M. Gisselbrecht, and C. L. Arnold, A high-repetition rate attosecond light source for time-resolved coincidence spectroscopy, Nanophotonics 10, 117 (2020).
- [52] S. Zhong, J. Vinbladh, D. Busto, R. J. Squibb, M. Isinger, L. Neoričić, H. Laurell, R. Weissenbilder, C. L. Arnold, R. Feifel, J. M. Dahlström, G. Wendin, M. Gisselbrecht, E. Lindroth, and A. L'Huillier, Attosecond electron-spin dynamics in Xe 4d photoionization, Nat. Commun. 11, 5042 (2020).
- [53] K. Henrichs, S. Eckart, A. Hartung, D. Trabert, K. Fehre, J. Rist, H. Sann, M. Pitzer, M. Richter, H. Kang, M. S. Schöffler, M. Kunitski, T. Jahnke, and R. Dörner, Multiphoton double ionization of helium at 394 nm: A fully differential experiment, Phys. Rev. A 98, 043405 (2018).
- [54] V. J. Montemayor and G. Schiwietz, Dynamic target screening for two-active-electron classical-trajectory Monte Carlo calculations for H⁺+ He collisions, Phys. Rev. A 40, 6223 (1989).
- [55] X. M. Tong and C. D. Lin, Empirical formula for static field ionization rates of atoms and molecules by lasers in the barriersuppression regime, J. Phys. B: At., Mol. Opt. Phys. 38, 2593 (2005).
- [56] R. Y. Rubinstein and D. P. Froese, *Simulation and the Monte Carlo Method*, 3rd ed. (Wiley, New Jersey, 2016).
- [57] B. Hu, J. Liu, and S. Chen, Plateau in above-threshold-ionization spectra and chaotic behavior in rescattering processes, Phys. Lett. A 236, 533 (1997).
- [58] N. B. Delone and V. P. Krainov, Tunneling and barriersuppression ionization of atoms and ions in a laser radiation field, Phys. Usp. 41, 469 (1998).
- [59] L. Fechner, N. Camus, J. Ullrich, T. Pfeifer, and R. Moshammer, Strong-field tunneling from a coherent super-

- position of electronic states, Phys. Rev. Lett. **112**, 213001 (2014).
- [60] D. C. Heggie, A global regularisation of the gravitational *N*-body problem, Celest. Mech. 10, 217 (1974).
- [61] P. Pihajoki, Explicit methods in extended phase space for inseparable Hamiltonian problems, Celest. Mech. Dyn. Astron. 121, 211 (2015).
- [62] L. Liu, X. Wu, G. Huang, and F. Liu, Higher order explicit symmetric integrators for inseparable forms of coordinates and momenta, Mon. Not. R. Astron. Soc. 459, 1968 (2016).
- [63] W. H. Press, S. A. Teukolsky, W. T. Vetterling, and B. P. Flannery, *Numerical Recipes: The Art of Scientific Computing*, 3rd ed. (Cambridge University Press, Cambridge, 2007).
- [64] R. Bulirsch and J. Stoer, Numerical treatment of ordinary differential equations by extrapolation methods, Numer. Math. 8, 1 (1966).
- [65] B. Eckhardt and K. Sacha, Classical threshold behaviour in a (1+1)-dimensional model for double ionization in strong fields, J. Phys. B: At., Mol. Opt. Phys. 39, 3865 (2006).
- [66] V. I. Arnold, Mathematical Methods of Classical Mechanics (Springer Science & Business Media, New York, 2013), Vol. 60
- [67] D. K. Efimov, J. S. Prauzner-Bechcicki, J. H. Thiede, B. Eckhardt, and J. Zakrzewski, Double ionization of a three-electron atom: Spin correlation effects, Phys. Rev. A 100, 063408 (2019).
- [68] D. K. Efimov, J. S. Prauzner-Bechcicki, and J. Zakrzewski, Strong-field ionization of atoms with p^3 valence shell: Two versus three active electrons, Phys. Rev. A **101**, 063402 (2020).
- [69] D. K. Efimov, A. Maksymov, J. Zakrzewski, and J. S. Prauzner-Bechcicki, Strong-field double ionization in a three-electron atom: Momentum-distribution analysis, Phys. Rev. A 108, 033103 (2023).
- [70] A. Chen, M. Kübel, B. Bergues, M. F. Kling, and A. Emmanouilidou, Non-sequential double ionization with near-single cycle laser pulses, Sci. Rep. 7, 7488 (2017).
- [71] J. S. Prauzner-Bechcicki, K. Sacha, B. Eckhardt, and J. Zakrzewski, Time-resolved quantum dynamics of double ionization in strong laser fields, Phys. Rev. Lett. 98, 203002 (2007).
- [72] B. Eckhardt, J. S. Prauzner-Bechcicki, K. Sacha, and J. Zakrzewski, Phase effects in double ionization by strong short pulses, Chem. Phys. 370, 168 (2010).
- [73] S. Majorosi, M. G. Benedict, and A. Czirják, Improved onedimensional model potentials for strong-field simulations, Phys. Rev. A 98, 023401 (2018).
- [74] V. S. Yakovlev, F. Bammer, and A. Scrinzi, Attosecond streaking measurements, J. Mod. Opt. 52, 395 (2005).
- [75] W. Becker, F. Grasbon, R. Kopold, D. B. Milošević, G. G. Paulus, and H. Walther, Above-threshold ionization: From classical features to quantum effects, Adv. At. Mol. Opt. Phys. 48, 35 (2002).